



Controllable formation of plasmonic gold nanoparticles by pulsed laser-induced etching

Walid K. Hamoudi¹ · Alwan M. Alwan¹ · Doaa Sulaiman¹

Received: 7 January 2020 / Accepted: 2 July 2020 / Published online: 9 July 2020
© Springer Science+Business Media, LLC, part of Springer Nature 2020

Abstract

This work discusses the preparation and formation of macro porous silicon (PSi) with silicon nano pillars; synthesized via laser-induced etching. The role of laser pulse duty cycle (10–100%) was investigated for silicon nano pillars samples creation using laser diode; characterized by its short wavelength (405 nm) and high laser intensity (500 mW/cm²). Morphological and spectroscopic aspects of the Si nanocrystallite sizes and plasmonic Au-NP, surface topography, roughness and thickness of the created layer were investigated by the scanning probe microscopy, photoluminescence measurements, the analysis of (FESEM) images and (XRD) patterns. The results revealed well-regulated Si nano pillars layers after adjusting the laser duty cycle under the same laser intensity and etching time. The histogram of Si nano pillars sizes, surface roughness and altitude of nano pillars within macro PSi created at 20% laser duty cycle showed specific characteristics; due to the minimal heat accumulation within the pillars and limited probability of damaging the pillars' morphological aspects. The Si nano pillars were employed to synthesize and control the plasmonic features of Au-NPs. The histogram of hotspot regions and plasmonic Au-NPs sizes and their specific surface areas and grain size showed well-controlled structures after adjusting the laser pulse duty cycle.

Keywords Pulsed laser · Porous silicon · Plasmonic · Nano pillars

1 Introduction

PSi is a complex silicon nanocrystallites matrix; prepared by etching silicon substrate in a hydrofluoric acid (HF) solution. Photochemical etching is one of most significant methods to control the density of silicon nanocrystallites (Hayder et al. 2016). In this method, the dissolution of silicon atoms within the HF solution is sustained by absorbing laser photons at the silicon layer surface (Alwan et al. 2015). PSi layer morphology, porosity and density of dangling bonds Si-H_x ($x = 1, 2, 3$) can be organized by specifying the experimental etching conditions; such as current density, time interval, laser intensity and laser

✉ Alwan M. Alwan
alkrzm@yahoo.com

¹ Department of Applied Science, Laser Science and Technology Division, University of Technology, Baghdad, Iraq

wavelength. The macro PSi is well-matched as an alternative element for chemical and biochemical sensors; especially when the Si nanocrystallites of the porous layer are uniformly distributed (Alwan et al. 2015; Huang et al. 2009). The use of short wavelength and high intensity continuous laser beam for silicon etching is capable of providing a high density of nucleation sites (dangling bonds) and the deposition of metallic nanoparticles within a specific size; due to the lower absorption depth (Kucherik et al. 2019). The drawback of this case, however, is the high probability of melting the Si nanocrystallites; due to heat accumulation that usually results from very low thermal conductivity (Yang and Minnich 2017). This necessitates a stringent laser illumination control during the etching (Huang et al. 2009). As a result, these effects could inhibit the formation of uniform Si nanocrystallites' sizes and morphological properties, hence; putting constrains on the use of this layer in PSi based nano photonics applications (Alwan et al. 2015). To overcome this problem, Hou et al., suggested that the use of a p-type silicon substrate with constant current variations in the electrochemical etching via positive pulses can retrieve the HF concentration within the pores and hence; improve the etching process (Xu et al. 2003a, b; Xiong et al. 1998). The formation of plasmonic nanoparticles within a specific size by dipping the Si nano-crystallites in an electrolytic solution represents as an efficient, simple and rapid process (Alexis et al. 2019). This is achieved through the ion reduction process by dangling bonds Si-Hx (x = 1, 2, 3) groups. At fixed electrolytic solution concentration and dipping period, the dangling bonds density and spatial distribution uniformity of the Si nano-crystallites act as important performers in the characteristics of metallic nanoparticles (Lannoo 1990; Alwan et al. 2017).

In this work, the laser duty cycle of laser-induced etching was investigated extensively to realize an optimum value at which the reaction between the HF solution and the silicon substrate is systematic. The idea was to fabricate an efficient Si nano pillars layer for nano photonic applications.

2 Experimental details

2.1 Formation of Si nano pillars layer

A mechanical chopper was assembled from low voltage dc motor and a number of circular discs of different square-shape apertures sizes. Each disc is attached to the motor's rotating axil at a time in order to control the laser duty cycles. The angular frequency of the rotating disc and hence; the laser pulse repetition rate were controlled by varying the applied voltage to the dc motor; which created a series of laser pulses at fixed laser intensity. The laser duty cycle pulse repetition rate was checked using a combination of optical detector and an oscilloscope. The macro-PSi of (Si nano pillars) samples were formed on two sided mirror-like n-type (100) oriented silicon substrate of 3–5 Ω -cm resistivity; using an etching solution consists of C₂H₅OH:HF 48% (2:1 by volume). The immersed silicon substrate was fixed on two Teflon pieces and laser-illuminated at normal incidence on the Si surface, in such a way that the internal photo current passes from non-illuminated lower Si surface to laser illuminated top surface through the electrolyte as illustrated in Fig. 1. In this electrode-free laser-induced etching method, no external voltage was applied. The 405 nm wavelength laser of 200 mW power was de-focused on the Si substrate to a circular spot of 1 cm² area to obtain a laser intensity of 500 mW/cm².

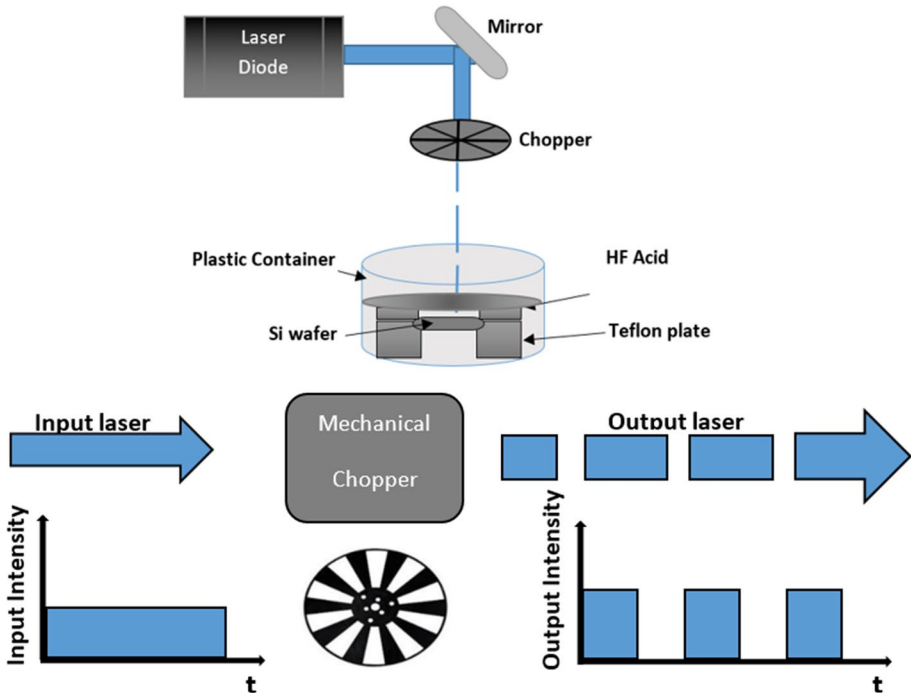


Fig. 1 Experimental set-up of laser-induced etching method

A series of Si nano pillars layers were obtained in dark at room temperature by using different duty cycles (10–100%). Etching factors are itemized in Table 1. In order to explore the morphology of the Si nano pillars' layers; prepared by laser-induced etching, the illumination period for every sample was varied. Keeping the internal charge transfer between the upper and lower surfaces for 10 min in the silicon sample S_1 equivalent to the samples prepared with continuous 500 mW/cm^2 illumination case, samples S_2 , S_3 , S_4 and S_5 were prepared by the duty cycles 10%, 20%, 30% and 40% of the sample S_1 respectively. The actual illumination period for all other samples; prepared at different duty cycles, is equivalent to 10 min as shown in Table 1.

The morphological aspects (Si nano pillars sizes and forms, surface topography, roughness and the altitude of Si nano pillars layer) were inspected by scanning probe microscopy (SPM); using contact mode type 400 AFM system. Besides; the spectroscopic aspects were studied from the photoluminescence PL spectra of the Si nano pillars samples; after

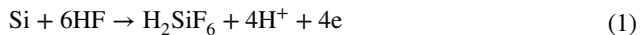
Table 1 Etching parameters for 500 mW/cm^2 laser intensity at different laser pulse duty cycles

Sample	Etching method	Total etching period (min)	Duty cycle (%)
S_1	Continuous illumination	10	100
S_2	Pulsed illumination	100	10
S_3	Pulsed illumination	50	20
S_4	Pulsed illumination	33	30
S_5	Pulsed illumination	25	40

employing CW 325 nm, 400 mW He-Cd laser of (PL) system from Horiba Jobin–Yvon T64000 spectrometer.

2.2 Formation of plasmonic Au-NPs/Si nano pillars layer

The regulatory of the morphological aspects of Si nano pillars layer is the most significant feature for adjusting the characteristics of Au-NPs. The plasmonic features of Au-NPs vary with nano pillars dimensions, form and the density, and surface roughness at fixed dipping condition. The Au-NPs/Si nano pillars layers were formed via passivation of the Au-NPs on Si nano pillars through the reduction of Au^{3+} to gold nanoparticles Au-NPs by easy and rapid dipping process. Different Si nano pillars were dipped in 5×10^{-3} M concentrations of (HAuCl_4) solution with a few drops of diluted 2.8 M of HF at a room temperature dipping period of 2 min. In gold dipping corroboration, the formation of Au-NPs on Si nano pillars surfaces takes place through the Volmer-Weber growth mechanism (Kaganer et al. 2009). Once a Si nano pillars sample is dipped in the HAuCl_4 solution, gold nanostructures is formed via gold ion reduction by means of the dangling bonds of the nano pillars. The density of these dangling bonds (nucleation sites) has a huge population at Si nano pillars. The gold nanostructures formation takes place according to the following equations (Alwan and Dheyab 2017):



Because of these reactions, gold nuclei and hence; the metal growth process, will occur at the surfaces of the nano pillars to create the macro PSi surface progressively via isolated and aggregated gold nanoparticles. At fixed dipping conditions, the metal growth process is affected by several significant factors such as density, type and locations of nucleation sites Si– H_x bonds (Makarov et al. 2014). The plasmonic features of Au-NPs/Si nano pillars were examined using (MIRA3 TESCAN) field–Emission scanning electron microscopy FE-SEM and X-ray diffraction (XRD-6000, Shemadzue), while Image-J software was employed to compute the Au-NPs size and hot spot histogram from the FE-SEM images.

3 Results and discussion

3.1 Characterization of silicon nano pillars

Figure 2a–f shows the SPM micro images of the samples S_2 , S_3 , S_4 , S_5 and S_1 . The 3-D micro images show that the surface of the silicon macro-PSi consists of Si nano pillars-like morphologies with different forms and sizes. These Si nano pillars are distributed randomly with different Si nano sizes. For the continuous illumination sample S_1 , (Fig. 2a), nano pillars-like structure was found to be most irregular with tendency of overlapping among the Si nano pillars. On the other hand, for macro-PSi prepared by utilizing laser pulses with duty cycles 10%, 20%, 30% and 40%, the silicon nano pillars had a tendency to be very well-organized and more uniformly distributed. Comparing between the 3-D micro images of the five samples, those created with 20% duty cycle (sample S_3 in Fig. 2c) revealed a highly uniform Si nano pillars aligned within

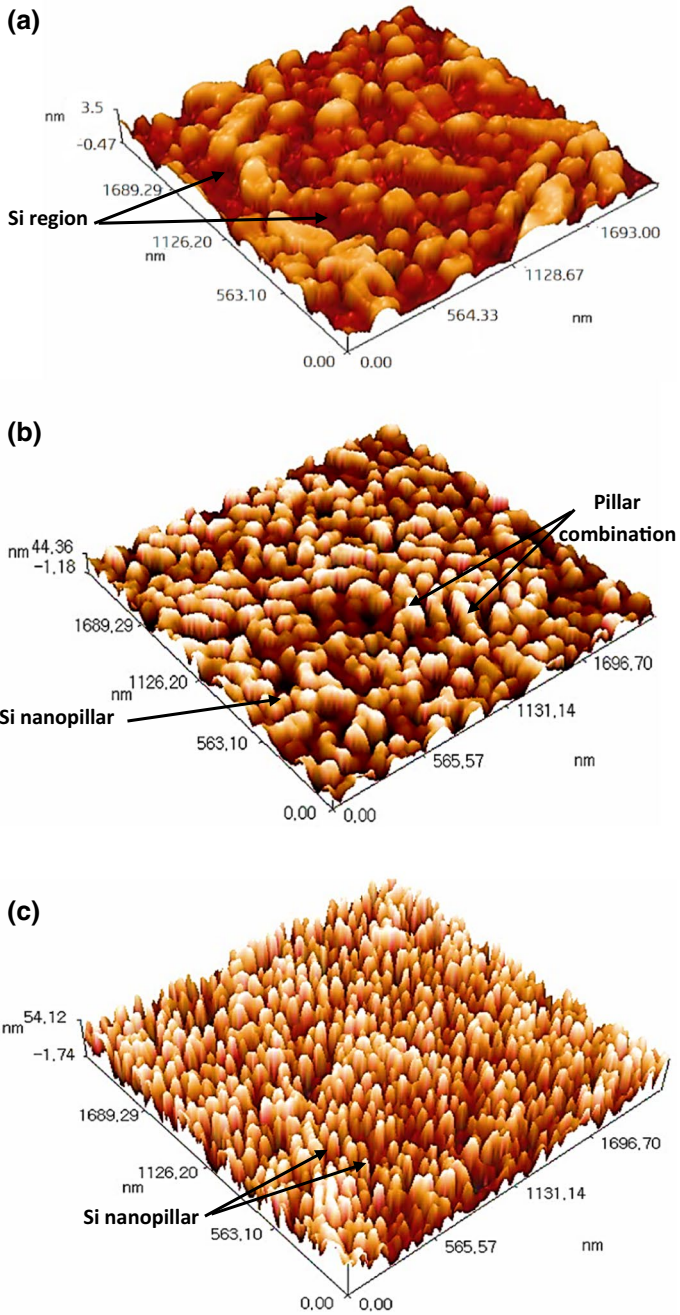


Fig. 2 SPM micro images of **a** continuous illumination sample and duty cycles pulsed illumination, samples: **b** 10%, **c** 20%, **d** 30% and **e** 40%

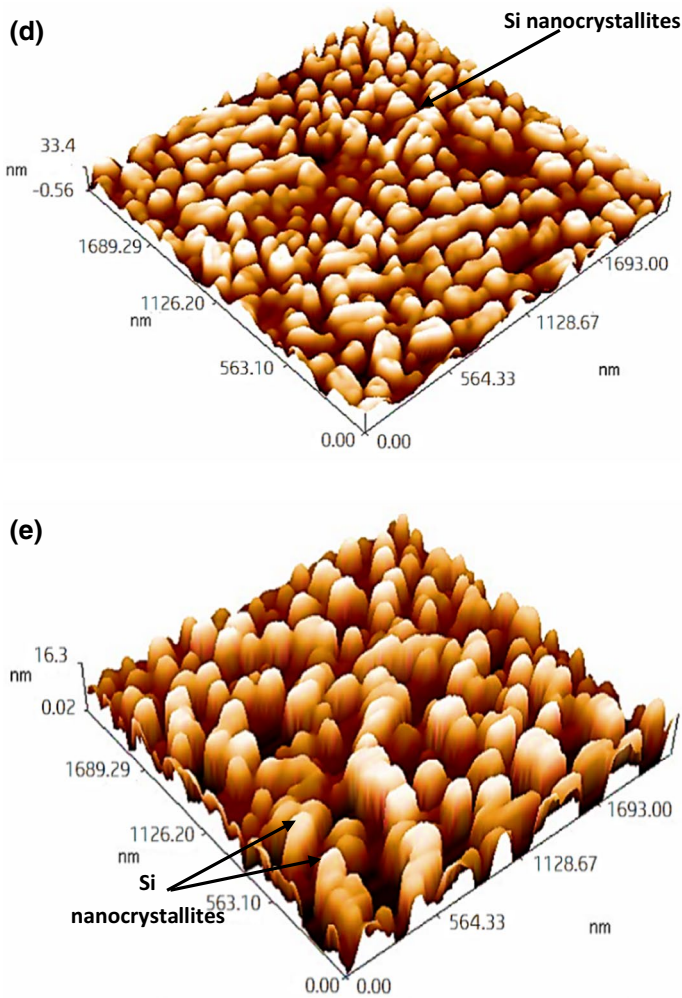


Fig. 2 (continued)

the macro-PSi layer. These dramatic variations in the surface morphologies of the Si nano pillars with the duty cycles are related with the photons absorption and hence; the photo-generated charge carriers within the silicon pillars. Greater duty cycles of the laser pulses can improve the Si etching rate and hence; the Si dissolution process. The internal charge transfer between the upper and lower surfaces in the silicon and hence; the initiated internal photo-current from the excessive duty cycles is given by (Alwan et al. 2015).

$$I_p = \frac{P(1-R)\eta}{hf} * e \quad (3)$$

where P is the incident optical power, R is a reflectivity of PSi surface, η is the quantum efficiency, f is the laser frequency, h is the Planck constant and e is the electric charge.

Based on Eq. (3), the absorbed laser intensity rises inside the macro-PSi and leads to an increase in the etching rate within the porous layer. One of main features of the etching process by short laser wavelength is the short absorption depth (equals the inverse of absorption coefficient). For 405 nm laser wavelength, the absorption depth is about 100 nm (Spinelli and Polman 2012), which means an efficient heating process within a small depth.

Besides; for greater duty cycles, the pillars heating increases and this in turn increases the temperature within the pillar matrix. The too low thermal conductivity 0.76 W/m/K of silicon nanocrystallite of sizes 100 to 300 nm as compared with that of bulk silicon 150 W/m/K (Chalhoub et al. 2011), will lead to increasing the probability of melting the Si nano pillars due to the heat accumulation within the pillars. This will push the probability of the overlapping process among the silicon nano pillars higher, which jeopardizes the morphological features of the macro-PSi.

The histogram for silicon nano pillars sizes as a function of duty cycles pulsed illumination is illustrated in Fig. 3a–e. For continuous illumination sample S_1 , Fig. 3a, the nano pillars diameter is ranging from 65 to 230 nm with an average diameter of 92.17 nm. For sample S_2 of lower 10% duty cycles, the nano pillars diameter is ranging from 50 nm

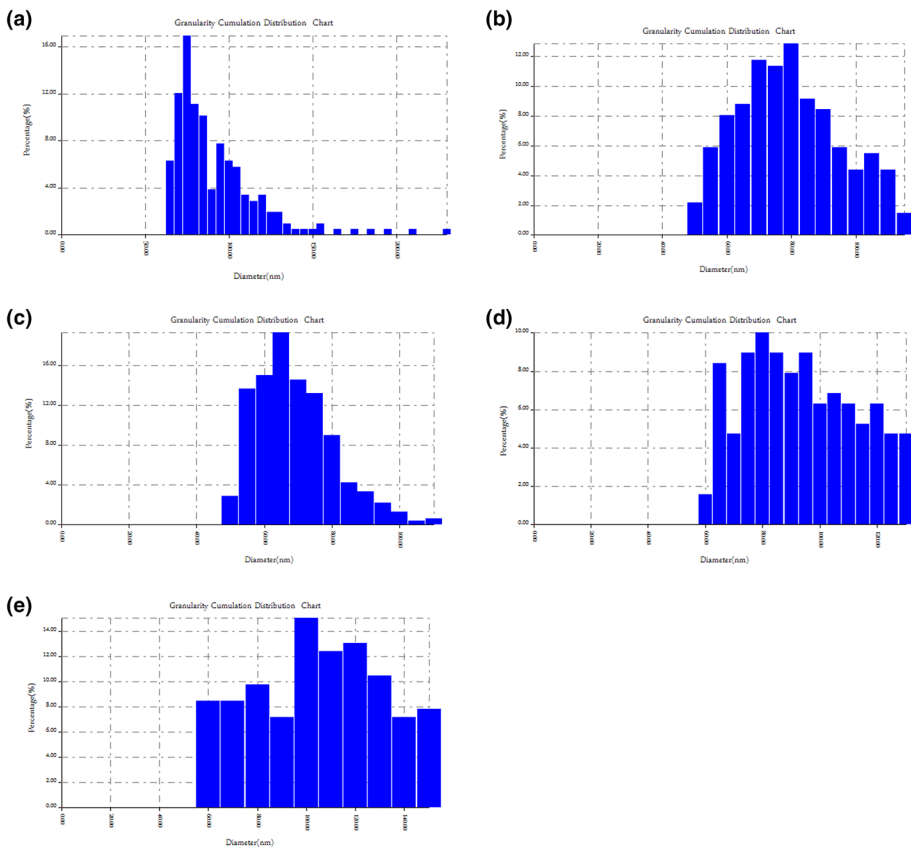


Fig. 3 Histogram of silicon nano pillars size for **a** continuous illumination sample S_1 , and duty cycles pulse illumination samples **b** 10%, **c** 20%, **d** 30% and **e** 40%

to 115 nm with an average diameter of 76.98 nm, Fig. 3b. By increasing the laser pulses duty cycles to 20%, sample S_3 , Fig. 3c, the nano pillars showed a diameter ranging from 45 to 110 nm with an average diameter of 65.6 nm. Further increase of the laser pulses duty cycles to 30% sample, S_4 , Fig. 3d, the to 150 nm range with an average diameter of 100 nm, as presented in Fig. 3e.

The average surface roughness and altitude of Si nano pillars samples as a function of laser pulses duty cycles are shown in Fig. 4. The average surface roughness varies with pulses duty cycles as shown in Fig. 4a. The surface roughness reaches a maximum value of about 13.6 nm for 20% pulses duty cycle for etched sample S_3 and a minimum value of about 1.8 nm for continuous illumination of the etched sample S_1 . The variations of the altitude of nano pillars with laser pulses duty cycles are illustrated in Fig. 4b. The highest value of nano pillars altitude 54 nm was obtained for 20% pulses duty cycle etched sample S_3 , whereas the lowest value 3.15 nm has resulted from continuous illumination etched sample S_1 . The reason behind this behavior could be due to the lower etching rate of the silicon surface in the x and y directions compared to the rate in the z-direction across the silicon layer. The etching rate of the S_3 sample showed the highest value for 20% pulses duty cycle among all other samples. Pulsating the continuous laser leads to increasing the altitude of the nano pillars within the limited 100 nm absorption depth. The values of average surface roughness and the depth of nano pillars within

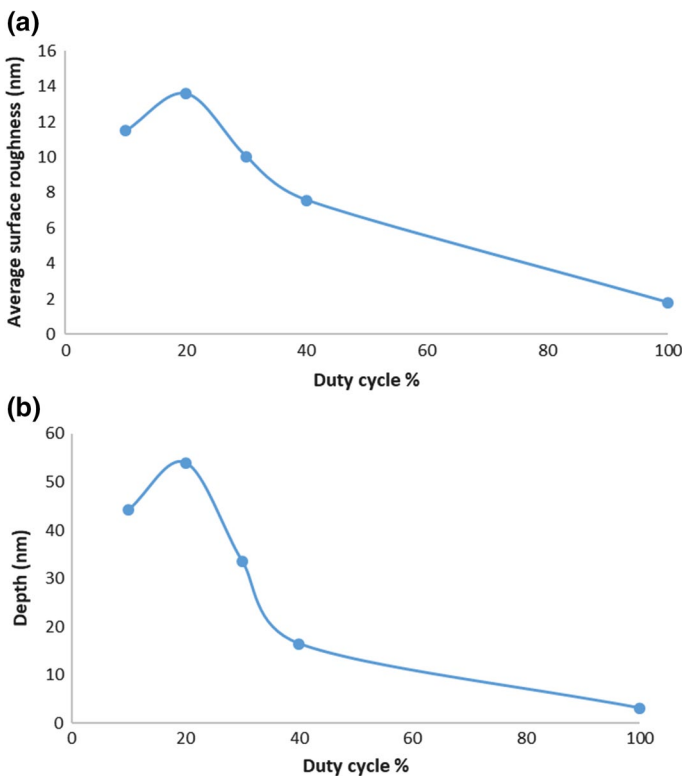


Fig. 4 Dependence of **a** average surface roughness and **b** altitude of Si nano pillars on the laser pulses duty cycles

the macro-PSi depth, reflect the finger print of that the density of dangling bonds Si-H_x (x = 1, 2, 3) groups; i.e. the nucleation sites of reducing the gold ions to gold nanoparticles.

The PL bands of the Si nano pillars samples for different laser pulses duty cycles within laser-induced etching process is shown in Fig. 5. For continuous illumination, etched sample S₁, the peak of PL spectrum is situated at 760 nm with 560 au. The role of laser pulses duty cycles on the PL spectrum is obviously experiential on both the wavelength peak location and the intensity of the PL bands. The effect of conversion the etching mode from continuous illumination mode to pulsing mode has led to a rise in the PL intensity with a blue shifting in the PL peak location. For laser pulses duty cycles of S₂ 10%, S₃ 20%, S₄ 30% and S₅ 40%, the PL peak location is 630, 600, 690 and 740 nm respectively, with their PL intensity of about 1650, 1850, 1050 and 850au.

The continuous illumination etched sample exhibited the lowest value of energy band gap of about E_g = 1.62 eV and the highest value of energy band gap of about 2.06 eV was obtained for sample of 20% pulses duty cycle in which Si nano pillars have lower dimensions.

The dependence of the PL spectrum of silicon nano-crystallites on the sizes of Si nano pillars is in an excellent agreement with the quantum confinement effect of charged carriers within the matrix of Si nano pillars (Kumar et al. 2013). The increasing of PL intensity is related to the density of Si nano pillars due to the radiative recombination process between electron and holes inside each pillar. The rise in the PL intensity is a finger print for the density of pillars (Sychugov et al. 2005).

The dependence of the dimension of nano pillar (nano wire) is given by the following equation (Pohl 2018)

$$E_{g(nanopillar)}(eV) = E_{g(bulkSi)} + \frac{h^2}{8} \left(\frac{1}{d_{(x)}} + \frac{1}{d_{(y)}} \right) \left[\frac{1}{m_e^*} + \frac{1}{m_h^*} \right] \tag{4}$$

where E_g (eV) is the PL peak position of nano pillar and the energy gap of bulk Si. E_g = 1.12 eV, h = 4.14 × 10⁻¹⁵ eV s is Planck's constant, m_e^{*} = 0.19m₀, m_h^{*} = 0.16m₀, and m₀ = 9.1 × 10⁻³¹ kg, d_(x) and d_(y) is the dimension of nano pillar.

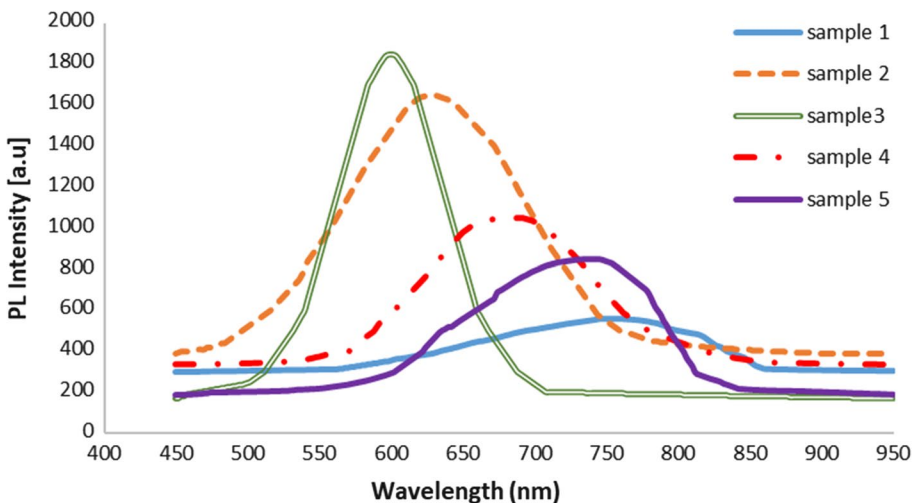


Fig. 5 PL bands of Si nano pillars layer within the macro-PSi

3.2 Morphological aspects of plasmonic Au-NPs/silicon nano pillars

Figure 6a–e, illustrates the incorporated Au-NPs; resulting from ion reduction process via nucleation sites Si–H_x bonds of Si nano pillars. Figure 6a, e, of continuous illumination sample and pulses duty cycles of 40% respectively, show a morphology of continuous layer covering over the Si nano pillars structures; subsequently from homogeneous growth, where the lower values of surface roughness, and the altitude of nano pillars refer to ion reduction process over silicon-rich with high density of (Si–H_x) bonds. The presence of

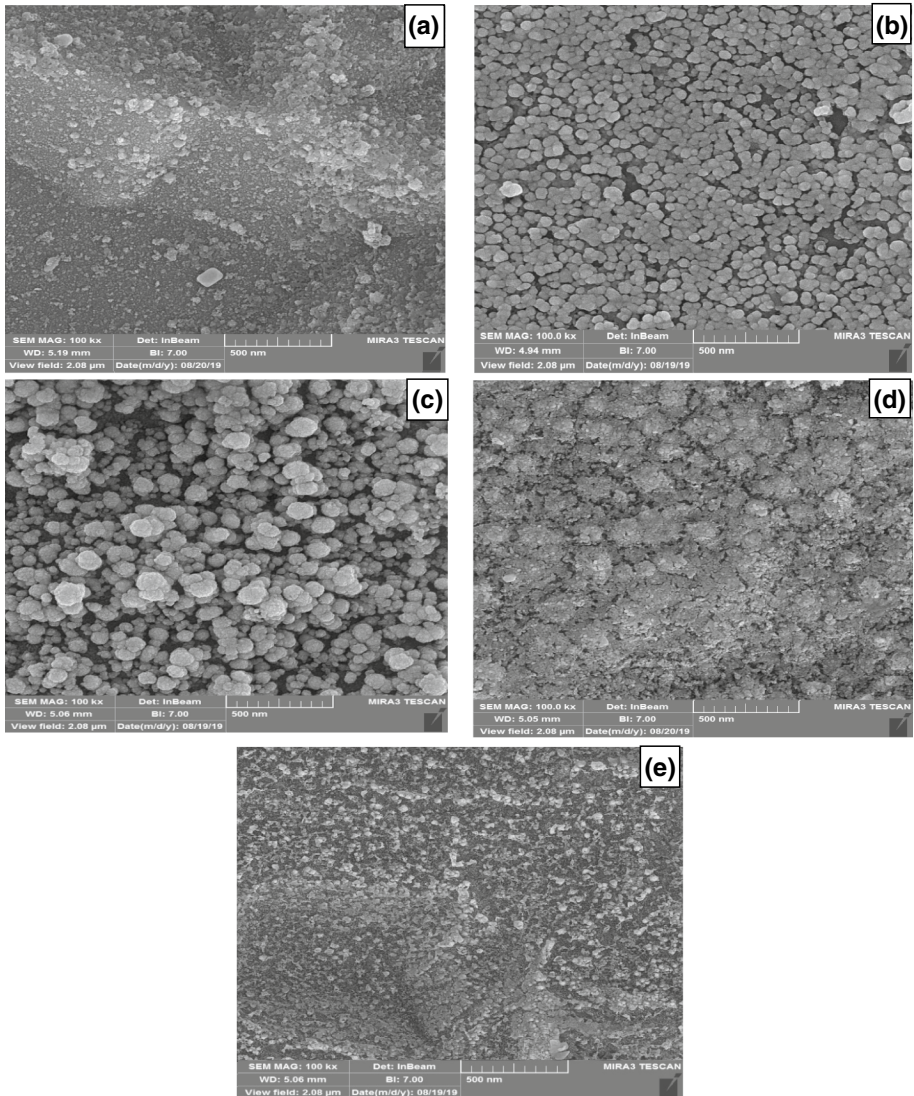


Fig. 6 SEM micro images of **a** continuous illumination sample S_1 and pulses duty cycles samples **b** 10%, **c** 30%, **d** 20% and **e** 40%

isolated semi-circular Au-NPs over the Si nano pillars is clearly shown in Fig. 6b of the sample prepared with 10% pulses duty cycles. This form of nanoparticles reflects a manner of very low aggregation tendency among the nanoparticles and the resulting incorporated layer for being just one layer. This behavior, in general, may be strongly related to the location of surface nucleation sites Si–H1 bonds above the apex of the resulting hillocks. Figure 6c is for the sample prepared with 20% pulses duty cycles at which the surface roughness and the altitude of nano pillars reached to maximum value. It is clear to us that the growth was dependent on Weber-Vomer mechanism. The form of the incorporated Au-NPs is semi-circular too but with significant degree of aggregation among the nanoparticles. This manner may, in general, be intensely connected to the presence of high degree dangling bonds (nucleation sites Si–H x ($x=2, 3$) groups) above the apex and on the surface of the resulting Si nano pillars. Finally, Fig. 6d for sample prepared with 30% pulses duty cycles, the formed Au-NPs is not completely covering the Si nano pillars layer; illustrating incomplete depletion of Si–H x ($x=2, 3$) groups throughout the growth process. The sizes of Au-NPs are greater than those in Fig. 6c; indicating a lower nucleation sites density than those prepared with 20% pulses duty cycles. This is attributed to the optimum values of the surface roughness and altitude of nano pillars. The resulting morphology of plasmonic Au-NPs completely varies with the topographical properties of the Si nano pillars.

The sizes of Au-NPs and hence; the scopes and density of hot spot regions among the formed nanoparticles vary with the topographical properties. Figures 7 and 8, illustrate the particle size and the hot spot region of continuous illumination sample and pulses duty cycles samples.

It is difficult to distinguish the dimension of the resulting Au-NPs for continuous illumination sample; Fig. 7a, as the Au-NPs cover the Si nano pillars structures and also difficult for sample 7e, with 40% pulses duty cycles due to the incomplete depletion of Si–H x

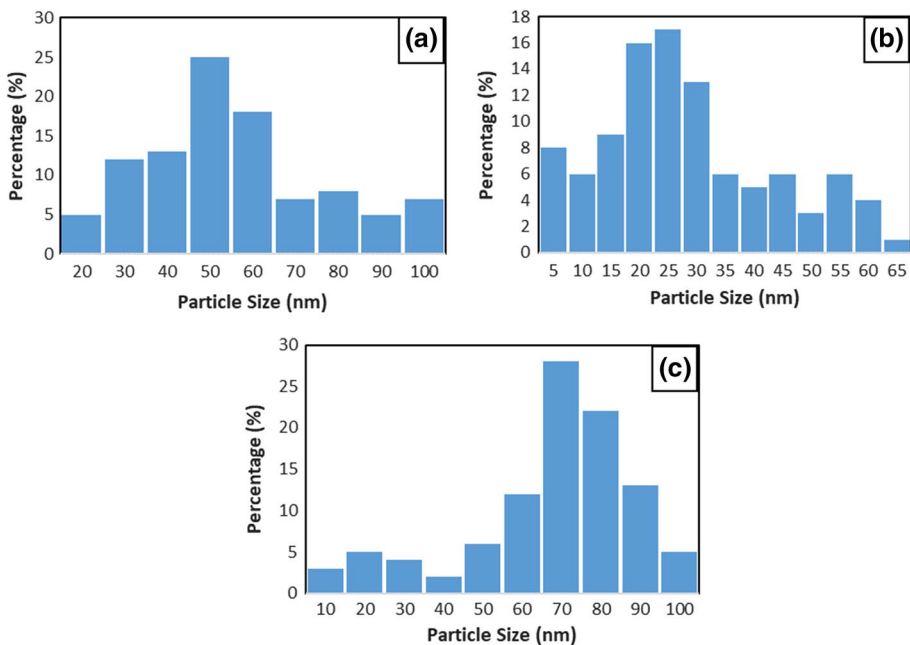


Fig. 7 histogram of Au-NPs size of **a** 10%, **b** 20%, **c** 30%

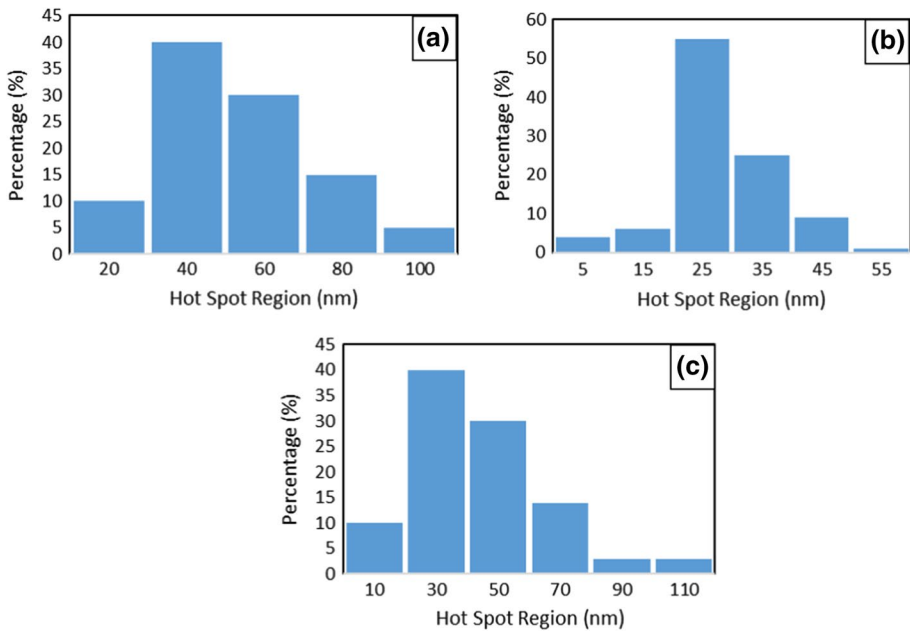


Fig. 8 Histogram of hot spot regions with pulses duty cycles samples **a** 10%, **b** 20%, **c** 30%

($x=2, 3$) groups. The histogram of Au-NPs with lower pulses duty cycles of about 10% Fig. 7b, varies from 20 to 100 nm, with peak at 50 nm. After increasing the laser pulses duty cycles to 20%, Fig. 7c, the histogram of the Au-NPs reached a minimum value ranging from 45 to 65 nm, with a peak located at 25 nm. Finally further increase of the pulse duty cycles to 30%; Fig. 5d, the Au-NPs sizes continue to rise, but with Au-NPs histogram fluctuating from 10 to 100 nm, with a peak situated at 70 nm.

Based on SEM micro images of continuous illumination sample and pulses duty cycles of 40%, the hot spot region is inattentive. This is because the plasmonic nanoparticles formed are deposited as a coating layer without any vacancies as a result of the lower value of the surface roughness (Hayder et al. 2016). The resulted hot spot region with 10% pulses duty cycles, Fig. 8a, is in the range between 20 and 100 nm with the highest peak at 40 nm. These regions are combinations of hot and cold nano-gaps. For 20% laser pulses duty cycles, Fig. 8b, the nano gap density in the resulted plasmonic Au-NPs was within the range 5–55 nm with its peak located at 25 nm. These hotspot regions are only hotspot regions. For sample with 30% laser pulses duty cycles, Fig. 8c, the sizes of the hot spot region among the plasmonic Au-NPs are ranging from 10 to 110 nm and the peak is at 30 nm. According to these values, this gap is again a combination of hot and cold nano-gaps. The above results infer that the plasmonic Au-NPs sizes can be considered as fingerprints of the features of Si nano pillars (surface roughness and altitude), where the greatest nucleation sites were contained at the high energy site such as the sharp nano pillars region (Zayer et al. 2019).

The EDX analysis of the plasmonic Au-NPs; incorporated on Si nano pillars, are illustrated in Fig. 9a–e. This figure approves the growth of gold nanoparticles and with the existence of only Si, without any additional elements. The peak intensity of plasmonic Au-NPs of continuous illumination sample and laser pulses duty cycles of 40% sample

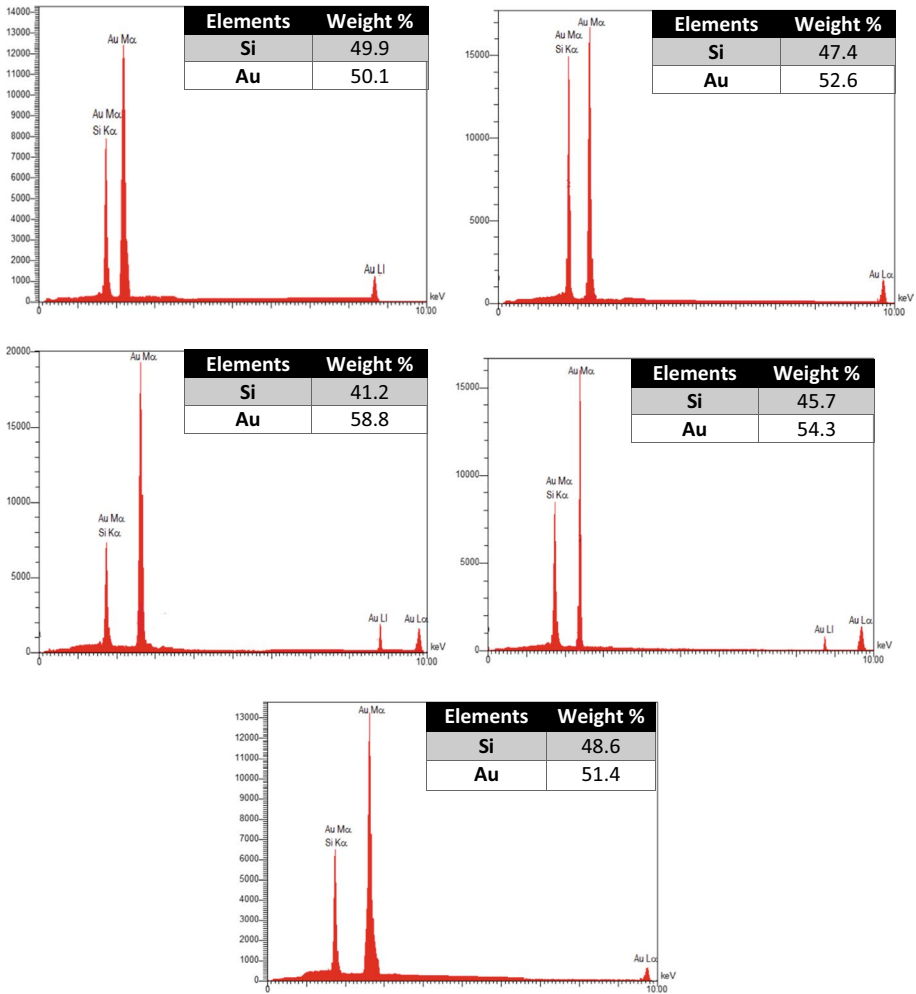


Fig. 9 EDX of **a** continuous illumination and pulses duty cycles samples **b** 10%, **c** 30%, **d** 20% and **e** 40%

(Fig. 9a, e) is higher than other samples; due to high ion reduction rate with (Si-H₁) bonds. The amount of the incorporated gold nanoparticles for the samples with other pulses duty cycles, Fig. 9b–d, have a comparable value because of similar ion reduction rate.

3.3 XRD pattern of plasmonic Au-NPs/Si nano pillars

Figure 10a–e shows the XRD pattern of Au-NPs/Si nano pillars prepared by incorporating Au-NPs on Si nano pillars samples with continuous illumination and with different laser pulses duty cycles of laser-induced etching. This figure shows that the Si nano pillars are still crystalline along the 100 plane at 2θ diffraction angle of around 33.5°, while the XRD of plasmonic Au-NPs shows particular Bragg's reflections at 2θ diffraction angles of around 38.2° and 44.3° for the planes 111 and 200. The variation of the laser duty cycles

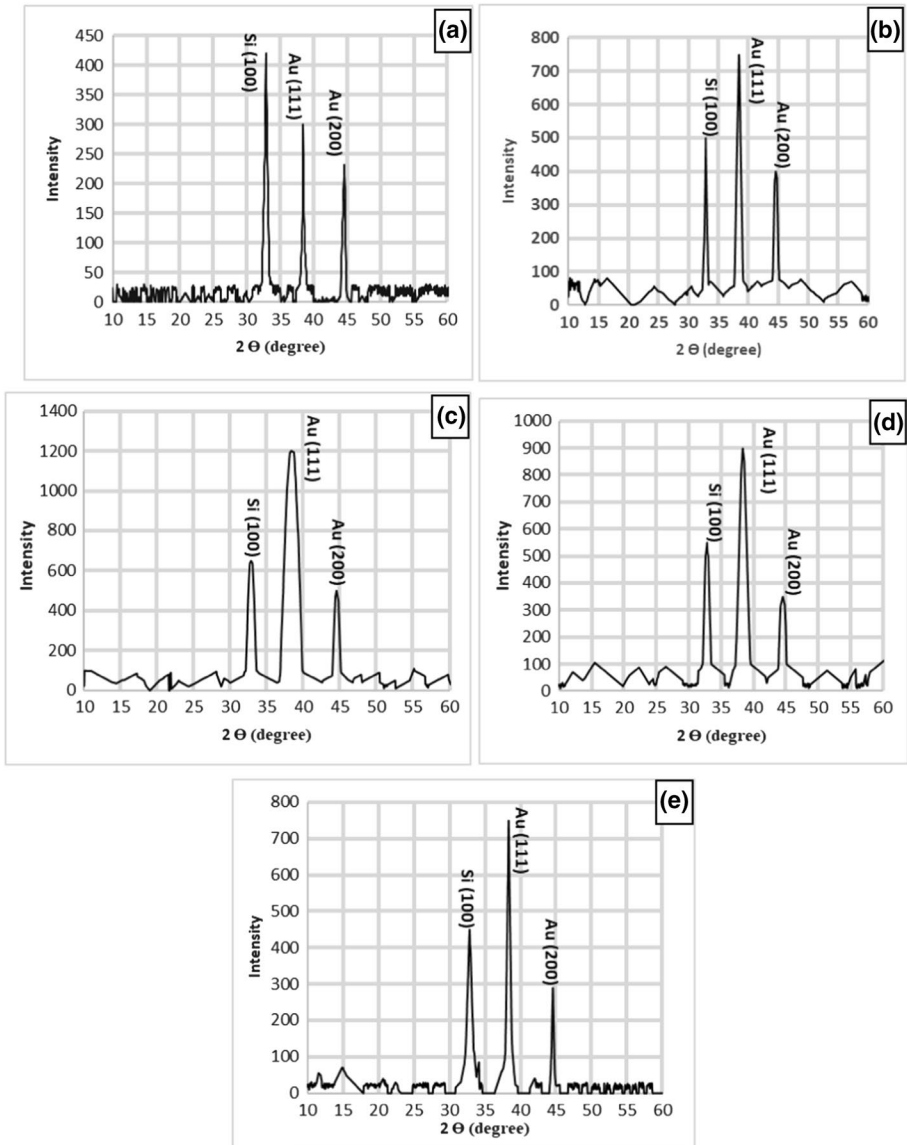


Fig. 10 XRD of **a** continuous illumination and pulses duty cycles samples **b** 10%, **c** 30%, **d** 20% and **e** 40%

leads to widening the full width half maximum (FWHM) of the Bragg's reflections. This behavior is mainly related to the sizes of the incorporated plasmonic Au-NPs. This small shift in Bragg's reflections (2θ) is due to the occurrence of local variation of interatomic space of the plasmonic Au-NPs Si nano pillars (Alwan et al. 2018). As the dimensions of the formed nanoparticles decrease, the (FWHM) of the diffraction becomes broader. As a result, the laser pulses duty cycles during laser-induced etching, will modify the sizes of Si nano pillars and hence; the formed plasmonic Au-NPs. The grain sizes of incorporated

plasmonic Au-NPs were computed from the Bragg's reflections broadening through the use of Scherer's formula (Zayer et al. 2019). The specific surface area (S.S.A.) is unique of the facts of the merit of plasmonic nanoparticles and specified by means of the following equation (Alwan et al. 2018):

$$S.S.A = \frac{6000}{D \cdot \rho} \quad (5)$$

where D and ρ are the grain size and the density of the plasmonic nanoparticles respectively.

The density of gold is about 19.3 g/cm^3 . Table 2 tabulates the values of Au-NPs grain sizes, (FWHM) of the Bragg's reflections, and specific surface area S.S.A. for plasmonic Au-NPs as a function of laser pulses duty cycles. Table 2 displays a maximum Au-NPs grain size of about 31.2 nm in the plane (111) for continuous 100% illumination. The minimum Au-NPs grain size in the plane (111) is about 3.6 nm for the sample with 20% laser pulses duty cycles. The maximum value of S.S.A for plasmonic Au-NPs of about $86.02 \text{ m}^2/\text{g}$ is for the sample with 20% laser pulses duty cycles while the minimum of about $9.96 \text{ m}^2/\text{g}$ is for the sample with 100% continuous illumination 100%. The decrease of plasmonic Au-NPs grain sizes and increase of S.S.A at fixed dipping condition of Si nano pillars into the HAuCl_4 solution can be clarified on the basis of the Si nano pillars features; especially the surface roughness and the altitude of base substrate.

4 Conclusions

In the current work, the alteration of surface topography as a function of laser pulses duty cycles in laser –induced etching; using short wavelength was studied. With specific value of laser pulses duty cycles, the optimum surface roughness, and altitude of the nano pillars were obtained. For continuous illumination, the silicon nano pillars were irregular, overlapped with large average diameter, but were very well-organized and uniformly distributed with smaller average diameter, when utilizing laser pulses; up to 30% duty cycles, with optimum at 20%. The absorbed laser intensity rises inside the macro-PSi leading to an increase in the etching rate within the porous layer. For larger duty cycles, the nano pillars heating increases leading to their melting and overlapping; a process that could jeopardize the macro-PSi morphology. Maximum surface roughness

Table 2 Au-NPs grain sizes, FWHM, and S.S.A. values of AuNPs formed at different laser pulses duty cycles

Duty Cycle	Plane (111)			Plane (200)		
	FWHM (rad)	Grain size of AuNPs (nm)	S.S.A of AuNPs (m^2/gm)	FWHM (rad)	Grain size of AuNPs (nm)	S.S.A of AuNPs (m^2/gm)
100	0.0047	31.2	9.96	0.0087	17.18	18.09
10	0.013	11.22	27.7	0.012	12.27	25.33
20	0.038	3.6	86.02	0.0149	10.11	30.74
30	0.024	6	51.8	0.0139	10.74	28.9
40	0.01	14.03	22.15	0.0088	17.03	18.254

and highest nano pillars altitude were seen for 20% pulses duty cycle and minimum values of these parameters have resulted for continuous illumination. The pulsing mode of illumination produced higher PL blue-shifted intensity and greater energy gap than the continuous illumination. Simple, cheap, rapid and well-organized approach for incorporating plasmonic Au-NPs (sizes and S.S.A.) on Si nano pillars was realized by controlling the laser pulses duty cycles during the etching process. The present results support the hypothesis and are within the context of the previous work. They make a valuable addition to this field. Further work of these new plasmonic Au-NPs will display a novel view for the potential of plasmonic devices.

References

- Alexis, L., Victoire, A., Boitel-Aullen, G., Mylan, L., Michèle, S., Souhir, B.: Silver-based plasmonic nanoparticles for and their use in biosensing. *Biosensors* **9**, 1–39 (2019)
- Alwan, A.M., Dheyab, A.B.: Room temperature CO₂ gas sensors of AuNPs/mesoPSi hybrid structures. *Appl. Nanosci.* **7**, 335–341 (2017)
- Alwan, A.M., Hayder, A.J., Jabbar, A.A.: Study on morphological and structural properties of silver plating on laser etched silicon. *Surf. Coat. Techbol.* **283**, 22–28 (2015)
- Alwan, A.M., Yousif, A.A., Wali, L.A.: A study on the morphology of the silver nanoparticles deposited on the n-type porous silicon prepared under different illumination types. *Plasmonics* (2017). <https://doi.org/10.1007/s11468-017-0620-3>
- Alwan, A.M., Rashid, R.B., Dheyab, A.B.: Morphological and electrical properties of gold nanoparticles/macro porous silicon for CO₂ gas. *Iraqi J. Sci.* **59**(1), 57–66 (2018)
- Chalhoub, A.E., Semmar, N., Coudron, L., Gautier, G., Boulmer-Leborgne, C., et al.: Thermal conductivity measurement of porous silicon by the pulsed-photothermal method. *J. Phys. D: Appl. Phys.* **44**, 1–16 (2011)
- Hayder, A.J., Alwan, A.M., Jabbar, A.A.: Optimizing of porous silicon morphology for synthesis of silver nanoparticles. *Microporous Mesoporous Mater.* **227**, 152–160 (2016)
- Huang, A.P., Uti, X.Y.J., Paul, K.C.: Surface modification of Si-based materials by plasma gas treatments. In: *Research Signpost*, pp. 335–387 (2009)
- Kaganer, V.M., Bernd, J., Roman, S., Wolfgang, B., Henning, R.: Kinetic optimum of volmer-weber growth. *Phys. Rev. Lett.* **102**, 1–14 (2009)
- Kucherik, A., Kutrovskaya, S., Osipov, A., Gerke, M., Chestnov, I., Arakelian, S., Shalin, A.S., Evlyukhin, A.B., Kavokin, A.V.: Nano-antennas based on silicon gold nanostructures. *Sci. Rep.* **9**(1), 1–6 (2019)
- Kumar, V., Saxena, K., Shukla, A.K.: Size-dependent photoluminescence in silicon nanostructures: quantum confinement effect. *Micro Nano Lett.* **8**(6), 311–314 (2013)
- Lannoo, M.: The role of dangling bonds in the properties of surfaces and interfaces of semiconductors. *Rev. Phys. Appl.* **25**, 887–894 (1990)
- Makarov, V.V., Love, A.J., Sinitysna, O.V., Makarova, S.S., Yaminsky, I.V., Taliany, M.E., Kalinina, N.O.: “Green” nanotechnologies: synthesis of metal nanoparticles using plants. *Acta Nat.* **6**, 35–44 (2014)
- Pohl, U.W.: *Low-Dimensional Semiconductors*. Springer Handbook of Materials Data, pp. 1081–1104 (2018)
- Spinelli, P., Polman, A.: Prospects of near-field plasmonic absorption enhancement in semiconductor materials using embedded Ag nanoparticles. *Opt. Express* **20**, 1–14 (2012)
- Sychugov, I., Juhasz, R., Linnros, J., Valenta, J.: Luminescence blinking of a Si quantum dot in a SiO₂ shell. *Phys. Rev. B* **71**, 115331–115335 (2005)
- Xiong, Z.H., Yuan, S., Jiang, Z.M., Qin, J., Peil, C.W., Liao, S., Ding, X.M., Hou, X.Y., Xun, W.: Photoluminescence studies of porous silicon microcavities. *J. Lumin.* **80**, 137–140 (1998)
- Xu, S.H., Xiong, Z.H., Gu, L.L., Liu, Y., Ding, X.M., Zi, J., Hou, X.Y.: Photon confinement in one-dimensional photonic quantum-well structures of nanoporous silicon. *Solid State Commun.* **126**, 125–128 (2003a)
- Xu, S.H., Xiong, Z.H., Gu, L.L., Liu, Y., Ding, X.M., Zi, J., Hou, X.Y.: Preparation of one-dimensional porous silicon photonic quantum-well structures. *Appl. Phys. A* **76**, 589–592 (2003b)

- Yang, L., Minnich, A.J.: Thermal transport in nanocrystalline Si and SiGe by ab initio based Monte Carlo simulation. *Sci. Rep.* **7**, 1–9 (2017). <https://doi.org/10.1038/srep44254>
- Zayer, M.Q., Alwan, A.M., Dheyab, A.B.: Optimizing of gold nanoparticles on porous silicon morphologies for a sensitive carbon monoxide gas sensor device. *Plasmonics* **14**(2), 501–509 (2019)

Publisher's Note Springer Nature remains neutral with regard to jurisdictional claims in published maps and institutional affiliations.